Boundary Element Analysis of Intracardiac Electrogram Sensing

John Alford*
Nick Cogan†
Charles Miller‡
Seth Patinkin§
Bradford E. Peercy¶
Noah A. Rosenberg||

August 5, 1998

Industry mentor: Dr. Shirley Min, Medtronic Inc.

*Department of Mathematics, University of Houston, Houston, TX
†Department of Mathematical Sciences, Montana State University, Bozeman, MT
‡Department of Mathematics, University of Notre Dame, Notre Dame, IN
§Department of Mathematics, Princeton University, Princeton, NJ
¶Department of Mathematics, University of Utah, Salt Lake City, UT
||Department of Biological Sciences, Stanford Unviversity, Stanford, CA

1 Introduction

Timely propagation of electrical signals is essential to proper functioning of the heart. Action potentials in the heart cause muscle contraction, which in turn governs blood circulation. Since action potentials can be measured by electrical sensing methods, sensing can help in diagnosing cardiac dysfunction.

An important action potential begins in the sino-atrial node above the atria and flows across the heart from the right atrium to the left. The action potential is enhanced by the atrio-ventricular node at the boundary of the atria and ventricles; it is propagated to the bottom of the heart, and finally it radiates throughout the ventricular myocardia.

1.1 Action Potentials in the Heart

At the cellular level, voltage-gated sodium ion (Na^+) channels located in cardiac cell membranes are responsible for the excitability of the tissue and thus, for the propagation of action potentials. Above a threshold concentration, the presence of sodium ions in the extracellular space causes a conformational change in the membrane proteins controlling the voltage-gated ion channels. The channels open, causing a further outflow of sodium ions into the extracellular space. Close proximity of channels and rapid diffusion cause efficient propagation of the action potential along the tissue. The efflux of the positive sodium ions from the more positively charged cells to the more negatively charged extracellular space creates an electric plane wave, which at each instant acts as a dipole source.

1.2 Electrode Sensing

Intracardiac electrodes entered through the veins into the right atrium or right ventricle sense the action potential against the endocardium of the atrium or ventricle. This method of sensing action potentials is less invasive than other intrathoracic methods of sensing. However, the proximity of the nearby ventricle to the atrial electrode causes interference with the signal. The action potential through the ventricles can be strong enough to register on an atrial electrogram. To avoid this oversensing and the possible misinterpretation of the signals as indicative of atrial fibrillation, we wish to better understand how the intracardiac electrodes sense the action potentials.

The sensing apparatus of the intracardiac electrodes consists of a metal tip separated by a length of insulation from a metal ring. The tip may be one of several shapes, such as hemispherical or cylindrical, and the ring is cylindrical. The difference in potential between the tip and the ring is the voltage measured in an electrocardiogram.

Our aim is to study the effect of the electrode geometry and the tip-to-ring spacing on the measured potential difference. With an ideal electrode geometry and spacing, we expect to record a high potential difference, highlighting the desired atrial signal compared to the interfering ventricular signal.

2 The Model - Homogeneous Medium

In this section, we develop an expression for the potential, considering a contribution to the potential from the charges induced by the dipole action potential on the electrodes. Sun and Min were among the first to consider the actual shape of the electrodes in deducing an expression for the potential, instead of treating the electrodes as points or using averaging techniques [6]. This paper uses the ideas of [6] to compare the effects of cylindrical and hemispherical tips and to study different tip-to-ring spacings.

2.1 The Integral Equation

For a given configuration of electrodes, the charge distribution in the myocardium induces charge distributions on the various electrodes. Thus, the electrostatic potential at an arbitrary point in space is affected by the charge distribution in the myocardium, as well as by the charge distributions induced on the conducting electrodes.

Using the continuity of current across cellular boundaries in the myocardium, Sun and Min derive an expression for the potential at an arbitrary point in terms of the unknown surface charge distributions on the electrodes [6]. We discuss aspects of the derivation of this integral equation, which we numerically solve for the surface charge distributions and for the potentials on the electrodes.

Following [6], we assume that a propagating wave in the myocardium can be represented as a dipole region D with continuous dipole moment volume density $\mathbf{P}$. The dipole moment volume density equals the current density generated by the cells of the myocardium. We also assume that the region outside the heart is a homogeneous medium described by two parameters: the conductivity σ and the permittivity ϵ.

At a point $\mathbf{r}$, the potential due to a point dipole at $\mathbf{r}'$ (in the myocardium) with dipole moment $\mathbf{p}$ is given by [3]

$$\phi(\mathbf{r}) = \frac{1}{4\pi\sigma}\frac{\mathbf{p}(\mathbf{r}')\cdot(\mathbf{r}-\mathbf{r}')}{|\mathbf{r}-\mathbf{r}'|^3}.$$

Analogously, the potential at $\mathbf{r}$ due to the continuous dipole distribution $\mathbf{P}(\mathbf{r}')$ is

$$\phi(\mathbf{r}) = \int_D \frac{1}{4\pi\sigma}\frac{\mathbf{P}(\mathbf{r}')\cdot(\mathbf{r}-\mathbf{r}')}{|\mathbf{r}-\mathbf{r}'|^3}d\mathbf{r}'.$$

Using the principle of superposition, the potential due to the induced charge distributions on the electrodes can be incorporated into the expression for the potential $\phi(\mathbf{r})$ by adding one term for each electrode. Since the electrodes are conductors, the induced charge in the interiors of the electrodes is zero.

Following [3], we derive the expression for the contribution to the potential from a surface charge distribution $\rho(\mathbf{r}')$ on a surface S. By Coulomb's law, the electric field at a point $\mathbf{r}$ is given by

$$\mathbf{E}(\mathbf{r}) = \oint_S \frac{1}{4\pi\epsilon}\frac{\rho(\mathbf{r}')(\mathbf{r}-\mathbf{r}')}{|\mathbf{r}-\mathbf{r}'|^3}dS.$$

Using the identity

$$\frac{\mathbf{r}-\mathbf{r}'}{|\mathbf{r}-\mathbf{r}'|^3} = -\nabla\left(\frac{1}{|\mathbf{r}-\mathbf{r}'|}\right)$$

where the gradient is taken with respect to $\mathbf{r}$, we can rewrite the expression for the electric field as

$$\mathbf{E}(\mathbf{r}) = -\oint_S \nabla\left(\frac{1}{4\pi\epsilon}\frac{\rho(\mathbf{r}')}{|\mathbf{r}-\mathbf{r}'|}\right)dS.$$

Since the gradient was with respect to $\mathbf{r}$, we can move the gradient outside the integral to obtain

$$\mathbf{E}(\mathbf{r}) = -\nabla\oint_S \frac{1}{4\pi\epsilon}\frac{\rho(\mathbf{r}')}{|\mathbf{r}-\mathbf{r}'|}dS.$$

The scalar electrostatic potential is defined by the equation $\mathbf{E}(\mathbf{r}) = -\nabla\phi(\mathbf{r})$, so that the potential from the surface charge distribution is

$$\phi(\mathbf{r}) = \oint_S \frac{1}{4\pi\epsilon}\frac{\rho(\mathbf{r}')}{|\mathbf{r}-\mathbf{r}'|}dS.$$

Finally, from a collection of E electrodes, the potential at $\mathbf{r}$ is

$$\phi(\mathbf{r}) = \sum_{i=1}^{E} \oint_{S_i} \frac{1}{4\pi\epsilon} \frac{\rho_i(\mathbf{r}')}{|\mathbf{r} - \mathbf{r}'|} dS_i$$

where S_i is the surface of the ith electrode and ρ_i is the charge distribution on S_i. Combining terms from the dipole distribution and from the electrodes, the potential at a point $\mathbf{r}$ is given by

$$\phi(\mathbf{r}) = \int_D \frac{1}{4\pi\sigma} \frac{\mathbf{P}(\mathbf{r}') \cdot (\mathbf{r} - \mathbf{r}')}{|\mathbf{r} - \mathbf{r}'|^3} d\mathbf{r}' + \sum_{i=1}^{E} \oint_{S_i} \frac{1}{4\pi\epsilon} \frac{\rho_i(\mathbf{r}')}{|\mathbf{r} - \mathbf{r}'|} dS_i. \tag{1}$$

In the above equation (1), the shape of the dipole region, the dipole distribution, the shapes and configuration of the electrodes, and the permittivity and conductivity of the medium are all known quantities. The surface charge distributions and the potential itself are unknown.

2.2 Boundary Conditions

To complete the statement of the model, we use the conducting nature of the electrode surfaces to provide boundary conditions for the unknown potential and the electrode surface charge distributions. For a given electrode surface S_i, constant potential V_i is maintained across the surface. The electrode surface is neutrally charged before being placed in the presence of the dipole source, and the redistribution of charge on the electrode surface does not change the fact that the total surface charge is zero. In other words, for $i = 1, \ldots, E$

$$\phi(\mathbf{r})|_{S_i} = V_i \tag{2}$$

$$\oint_{S_i} \rho_i(\mathbf{r}) dS_i = 0. \tag{3}$$

2.3 General Theory of the Method of Moments

The method of moments is a procedure for solving an inhomogeneous equation $L(f) = g$, where L represents a known linear operator, f is an unknown function, and g is a known function. To implement the procedure, we first choose a linearly independent collection of basis functions f_n, and we express f as a linear combination of these basis functions:

$$f = \sum_{n=1}^{N} \alpha_n f_n.$$

Note that the expansion is approximate, and to obtain a closer approximation to f we must increase N. We then select M linearly independent weighting functions w_m and take the inner product of the above equation with the weighting functions:

$$\sum_{n=1}^{N} \alpha_n < w_m, L(f_n) > = < w_m, g >, \; m = 1, 2, \ldots, M.$$

Denoting the coefficient $< w_m, L(f_n) >$ by l_{mn}, we now have a system of M linear equations in the N unknowns $\alpha_n, n = 1, \ldots, N$. In matrix form,

$$[l_{mn}][\alpha_n] = [g_m].$$

where $[l_{mn}]$ is the matrix of known inner products, $[\alpha_n]$ is the vector of unknowns, and the elements of $[g_m]$ are given by $g_m = < w_m, g >$.

If we choose $M = N$ we can solve the system for $[\alpha_n]$, and we obtain an approximate solution for the unknown function f. To obtain a nearer approximation to the actual function, we choose a larger collection of basis functions and weighting functions. A more complete description of the method of moments is provided by [1].

2.4 Application of the Method of Moments to the Model

In order to adapt our problem of computing the unknown surface charge densities ρ_i and the unknown potential $\phi(\mathbf{r})$, we must write our equation in the form $L(f) = g$. We must also select suitable basis functions and weighting functions.

Since sensing takes place on the electrodes, the particular electrostatic potentials of interest are the values of V_i on the E different electrode surfaces. Let $\rho(\mathbf{r}')$ be defined on $\cup_{i=1}^{E} S_i$ by $\rho(\mathbf{r}') = \rho_i(\mathbf{r}')$ whenever $\mathbf{r}'$ is in S_i. Let $V(\mathbf{r}')$ be similarly defined on $\cup_{i=1}^{E} S_i$ by $V(\mathbf{r}') = V_i(\mathbf{r}')$ whenever $\mathbf{r}'$ is in S_i.

Equations (1), (2), and (3) provide us with a collection of $2E$ equations in the $2E$ unknowns $\rho_1, \ldots, \rho_E$ and $V_1, \ldots, V_E$. In order to construct the equations, we express equation (1) using simpler notation. Denote by K_i the linear operator which takes a charge distribution as input and computes at a point $\mathbf{r}$

$$K_i(\rho(\mathbf{r})) = \oint_{S_i} \frac{\rho_i(\mathbf{r}')}{4\pi\epsilon|\mathbf{r} - \mathbf{r}'|}\, dS_i.$$

Also, let

$$q(\mathbf{r}) = -\int_D \frac{1}{4\pi\sigma} \frac{\mathbf{P}(\mathbf{r}') \cdot (\mathbf{r} - \mathbf{r}')}{|\mathbf{r} - \mathbf{r}'|^3}\, d\mathbf{r}'. \tag{4}$$

Expressed in terms of K and q, equation (1) becomes

$$\phi(\mathbf{r}) = -q(\mathbf{r}) + \sum_{i=1}^{E} K_i(\rho_i(\mathbf{r})).$$

If $\mathbf{r}$ is on the lth surface, applying the boundary condition from (2), the above equation simplifies to a linear equation in the variables $\rho_1, \ldots, \rho_E$ and V_k:

$$q_l(\mathbf{r}) = -V_l + \sum_{i=1}^{E} K_{i,l}(\rho_i(\mathbf{r})). \tag{5}$$

In the above equation (5), $q_l(\mathbf{r})$ is the same as the function $q(\mathbf{r})$, except that the allowable values of $\mathbf{r}$ are restricted to S_l. Similarly, $K_{i,l}$ is the same as K_i, except that the allowable values $\mathbf{r}$ are restricted to S_l. Applying equation (2) for each S_l, we obtain E linear equations.

Now we define T_i to be the linear operator which takes a charge distribution as input and computes $T_i(\rho) = \oint_{S_i} \rho(\mathbf{r}')\, dS_i$. Applying equation (3) E times, we obtain E linear equations. For each i, $i = 1, 2, 3, \ldots, E$

$$T_i(\rho_i) = 0.$$

Collecting the $2E$ equations into matrix form, we obtain the following linear system to solve for $\rho_1, \ldots, \rho_E$ and $V_1, \ldots, V_E$

$$\left(\begin{array}{ccc|ccc} K_{11} & \cdots & K_{1E} & -1 & \cdots & 0 \\ \vdots & & \vdots & \vdots & & \vdots \\ K_{1E} & \cdots & K_{EE} & 0 & \cdots & -1 \\ \hline T_1 & \cdots & 0 & 0 & \cdots & 0 \\ \vdots & & \vdots & \vdots & & \vdots \\ 0 & \cdots & T_E & 0 & \cdots & 0 \end{array}\right)\left(\begin{array}{c} \rho_1 \\ \vdots \\ \rho_E \\ \\ V_1 \\ \vdots \\ V_E \end{array}\right) = \left(\begin{array}{c} q_1 \\ \vdots \\ q_E \\ \\ 0 \\ \vdots \\ 0 \end{array}\right)$$

Denoting the matrix by L and the vector on the right by g, we now have $L\begin{pmatrix} \rho(\mathbf{r}) \\ V(\mathbf{r}) \end{pmatrix} = g(\mathbf{r})$, the appropriate form for applying the method of moments. We are now ready to select our basis functions and our weighting functions.

2.4.1 Expressing K in terms of basis functions: the upper left block

Partition the surface S_i into a collection of N_i disjoint surface elements $\sigma_{i,n}$. Let $\rho_{i,n}(\mathbf{r}')$ be the characteristic function of the region $\sigma_{i,n}$. The collection of these characteristic functions constitutes a linearly independent set, and the functions serve as our choice for the basis functions. The charge density ρ can be expressed as a linear combination of these characteristic functions:

$$\rho = \sum_{i=1}^{E}\sum_{n=1}^{N_i} \alpha_{i,n}\rho_{i,n}.$$

For the weighting functions, we select $w_{j,m} = \delta(\mathbf{r} - \mathbf{r_{j,m}})$ where $\mathbf{r_{j,m}}$ is the center of the mth surface element on the jth surface. For the rest of the derivation, note that the indices j and m and the variable $\mathbf{r}$ relate to the point at which charge is sensed, while the indices i and n and the variable $\mathbf{r}'$ relate to the source of the sensed charge.

We define an inner product

$$< u(\mathbf{x}), v(\mathbf{x}) >= \int_{R^3} u(\mathbf{x})v(\mathbf{x})\ d\mathbf{x}.$$

As m travels over the jth surface, we use equation (4) and the fact that the upper E components of the function g equal $q_1, q_2, \ldots, q_E$ to show that when g is expanded,

$$g_{j,m} =< w_{j,m}, g >= \int_{R^3} \delta(\mathbf{r} - \mathbf{r_{j,m}})g(\mathbf{r})\ d\mathbf{r} = -\int_D \frac{P(\mathbf{r}')\cdot(\mathbf{r_{j,m}} - \mathbf{r}')}{4\pi\sigma|\mathbf{r_{j,m}} - \mathbf{r}'|^3}\ d\mathbf{r}'.$$

The value of $k_{(j,m),(i,n)}$, the matrix element in the mth row and nth column of the K_{ji} block of the operator matrix, is

$$\begin{aligned} k_{(j,m),(i,n)} &=< w_{j,m}, L(\rho_{i,n}) > \\ &=< \delta(\mathbf{r} - \mathbf{r_{j,m}}, L(\rho_{i,n}(r')) > \\ &= \int_{R^3} \delta(\mathbf{r} - \mathbf{r_{j,m}})[\oint_{S_i} \tfrac{\rho_{i,n}(\mathbf{r}')}{4\pi\epsilon|\mathbf{r}-\mathbf{r}'|}d\sigma_{i,n}]\ d\mathbf{r} \\ &= \oint_{S_i} \tfrac{\rho_{i,n}(\mathbf{r}')}{4\pi\epsilon|\mathbf{r_{j,m}}-\mathbf{r}'|}d\sigma_{i,n} \\ &= \oint_{\sigma_{i,n}} \tfrac{1}{4\pi\epsilon|\mathbf{r_{j,m}}-\mathbf{r}'|}d\sigma_{i,n} \end{aligned}$$

The conclusion of this discussion, namely that

$$k_{(j,m),(i,n)} = \oint_{\sigma_{i,n}} \frac{1}{4\pi\epsilon|\mathbf{r_{j,m}} - \mathbf{r}'|}\, d\sigma_{i,n} \tag{6}$$

provides us with a method for determining the upper left block of the matrix L. Each column of the block corresponds to integrating over a particular surface element of a particular surface; each row of the block corresponds to the contribution to the potential at a point $\mathbf{r_{j,m}}$. Notice that this block is neither symmetric nor sparse. Each element is obtained from a different integral, we do not expect any of the integrals to be zero. Notice also that the diagonal elements may be problematic since they involve integrals where the observation point $\mathbf{r_{j,m}}$ lies in the region $\sigma_{i,n}$.

2.4.2 Expressing T in terms of basis functions: the lower left block

The operator T_i simply integrates ρ_i over the surface S_i. When we expand ρ_i using basis elements, the matrix representation of the operator T_i must incorporate the areas of the various basis elements. Letting $A(\sigma_{i,n})$ denote the area of a patch $\sigma_{i,n}$, the operator T_i expands into a vector $(A(\sigma_{i,1}), A(\sigma_{i,2}), \ldots, A(\sigma_{i,N_i}))$.

2.4.3 The right blocks of the matrix equation

When ρ_i is expanded using basis elements, V_i must be subtracted for each basis element. Thus, each -1 in the upper right block of the matrix equation expands into a vector of -1s.

The lower right block of the matrix equation is expanded to the appropriate dimensions and we fill the block with zeroes.

2.4.4 The matrix equation written out in all its glory

For a model with two electrodes ($E = 2$), the expansion of the matrix of operators via the moment of methods provides:

$$\left(\begin{array}{ccccccc|cc}
\multicolumn{6}{c|}{k_{(j,m),(i,n)} = \oint_{\sigma_{i,n}} \frac{1}{4\pi\epsilon|\mathbf{r_{j,m}}-\mathbf{r}'|} d\sigma_{i,n}} & & -1 & 0 \\
 & & & & & & \vdots & \vdots \\
 & & & & & & -1 & 0 \\
 & & & & & & 0 & -1 \\
 & & & & & & \vdots & \vdots \\
 & & & & & & 0 & -1 \\
\hline
A(\sigma_{1,1}) & \cdots & A(\sigma_{1,N_1}) & 0 & \cdots & 0 & 0 & 0 \\
0 & \cdots & 0 & A(\sigma_{2,1}) & \cdots & A(\sigma_{2,N_2}) & 0 & 0
\end{array}\right)
\left(\begin{array}{c} \alpha_{1,1} \\ \vdots \\ \alpha_{1,N_1} \\ \alpha_{2,1} \\ \vdots \\ \alpha_{2,N_2} \\ \hline V_1 \\ V_2 \end{array}\right)
=
\left(\begin{array}{c} g_{1,1} \\ \vdots \\ g_{1,N_1} \\ g_{2,1} \\ \vdots \\ g_{2,N_2} \\ \hline 0 \\ 0 \end{array}\right)$$

2.4.5 Computation of representation of K operator for a cylindrical charge source

To evaluate $k_{(j,m),(i,n)}$ in the case that S_i is a cylindrical surface, we let the patches $\sigma_{i,n}$ be described by intervals in the angular coordinate and the height. The point $\mathbf{r_{j,m}}$ lies at the center of the patch labeled m on the jth surface.

Using cylindrical coordinates, we denote the position of $\mathbf{r_{j,m}}$ by $(R_{j,m}, \theta_{j,m}, z_{j,m})$. In the integration from equation (6), the variable $\mathbf{r}'$ traverses the cylinder. We parametrize the position of $\mathbf{r}'$ by $\mathbf{r}' = (R_1, \theta', z')$, where R_1 is the radius of the cylinder.

The differential in our coordinate system is

$$d\sigma_{i,n} = R_1 d\theta' dz'.$$

Using the distance formula in cylindrical coordinates, we substitute into equation (6) to obtain

$$k_{(j,m),(i,n)} = \int_{\theta_{i,n}}^{\theta_{i,n+1}} \int_{z_{i,n}}^{z_{i,n+1}} \frac{R_1 d\theta' dz'}{4\pi\epsilon\sqrt{R_{j,m}^2 + +R_1^2 - 2R_{j,m}R_1 cos(\theta_{j,m} - \theta') + (z_{j,m} - z')^2}}.$$

2.4.6 Computation of representation of K operator for a hemispherical charge source

To evaluate $k_{(j,m),(i,n)}$ in the case that the charge source S_i is a hemispherical surface, we let the patches $\sigma_{i,n}$ be described by intervals in both angular coordinates. The point $\mathbf{r_{j,m}}$ lies at the center of the patch labeled m on the jth surface.

Using spherical coordinates, we denote the position of $\mathbf{r_{j,m}}$ by $(R_{j,m}, \theta_{j,m}, \Phi_{j,m})$. In the integration from equation (6), the variable $\mathbf{r}'$ traverses the hemisphere. We parametrize the position of $\mathbf{r}'$ by $\mathbf{r}' = (R_2, \theta', \Phi')$, where R_2 is the radius of the hemisphere.

The differential in our coordinate system is

$$d\sigma_n = R_2^2 \sin(\Phi') d\theta' d\Phi'.$$

Using the distance formula in spherical coordinates, we substitute into equation (6) to obtain

$$k_{(j,m),(i,n)} = \int_{\theta_{i,n}}^{\theta_{i,n+1}} \int_{\Phi_{i,n}}^{\Phi_{i,n+1}} \frac{R_2^2 \sin(\Phi') d\theta' d\Phi'}{4\pi\epsilon\sqrt{F}}$$

where

$$F = R_{j,m}^2 + R_2^2 - 2R_{j,m}R_2[\sin(\Phi_{j,m})\sin(\Phi')[\cos(\theta_{j,m} - \theta')] + \cos(\Phi_{j,m})\cos(\Phi')].$$

3 The Model - Inhomogeneous Medium

In this section, we consider a generalized version of the earlier model. We assume that the blood and myocardium are two different homogeneous media, separated by a plane interface. With this formulation, the traveling pulse in the heart is contained fully within the myocardium, while the electrodes are contained fully within the blood. As in the previous problem, the pulse induces surface charge distributions on the various electrodes. However, because of the inhomogeneity of the medium, charge builds up at the interface between the blood and the myocardium. The normal components of the electric fields on opposite sides of the boundary are not identical, and in accordance with Gauss's law, a surface charge density proportional to the field difference accumulates at the boundary [3]. This charge density provides an extra complication which must be incorporated into the expression for the potential.

3.1 The Operator Matrix

Suppose that we have E electrode surfaces S_1 through S_E, a dipole source in the myocardial tissue D, and an interface between inhomogeneous media Γ. For convenience, call the blood region B and the myocardial tissue region through which the electrical plane wave travels M. Furthermore, let σ_+ and ϵ_+ represent the conductivity and permittivity of B, respectively. Similarly, let σ_- and ϵ_- represent the conductivity and permittivity of M.

Jumping straight to the operator matrix, the similarity of notation and matrix structure to those of the homogeneous problem suggest the derivation that follows in subsection 3.4. Collecting $2E+1$ equations into matrix form, we have the following linear system to solve for $\rho_1, \ldots, \rho_E$, η, and $V_1, \ldots, V_E$.

$$\left(\begin{array}{ccc|c|ccc} \frac{\partial}{\partial \mathbf{n}}({K_1}^{+,-}) & \cdots & \frac{\partial}{\partial \mathbf{n}}({K_E}^{+,-}) & \frac{\partial}{\partial \mathbf{n}}({M}^{+,-}) & 0 & \cdots & 0 \\ {K_{1,1}}^{+} & \cdots & {K_{E,1}}^{+} & {M_1}^{+} & -1 & \cdots & 0 \\ \vdots & & \vdots & \vdots & \vdots & & \\ {K_{1,E}}^{+} & \cdots & {K_{E,E}}^{+} & {M_E}^{+} & 0 & \cdots & -1 \\ T_1 & \cdots & 0 & 0 & 0 & \cdots & 0 \\ \vdots & & \vdots & \vdots & \vdots & & \\ 0 & \cdots & T_E & 0 & 0 & \cdots & 0 \end{array}\right) \left(\begin{array}{c} \rho_1 \\ \vdots \\ \rho_E \\ \eta \\ V_1 \\ \vdots \\ V_E \end{array}\right) = \left(\begin{array}{c} 0 \\ -{J_1}^{+} \\ \vdots \\ -{J_E}^{+} \\ 0 \\ \vdots \\ 0 \end{array}\right)$$

Denoting the matrix by L_{inh} and the vector on the right by g, we now have $L_{inh} \begin{pmatrix} \rho(\mathbf{r}) \\ \eta(\mathbf{r}) \\ V(\mathbf{r}) \end{pmatrix} = g(\mathbf{r})$. We will apply the method of moments to each of the $E^2 + 3E + 1$ different operators in the matrix. The resulting linear system can be solved as done with the homogeneous model to obtain approximations of the unknown surface charges and potentials. Though we have not yet defined these operators in full, it should be observed that the essence of the inhomogeneity is captured in the first row of L_{inh}.

3.2 The Operators

By superposition, we obtain two following potential equations, where ρ_i represents the charge density on the electrode surface and η respresents the charge density on the interface:

$$\phi^+(\mathbf{r}) = \int_D \frac{1}{4\pi\sigma_+}\frac{\mathbf{P}(\mathbf{r}')\cdot(\mathbf{r}-\mathbf{r}')}{|\mathbf{r}-\mathbf{r}'|^3}d\mathbf{r}' + \sum_{i=1}^{M}\oint_{S_i}\frac{1}{4\pi\epsilon_+}\frac{\rho_i(\mathbf{r}')}{|\mathbf{r}-\mathbf{r}'|}dS_i + \oint_\Gamma \frac{1}{4\pi\epsilon_+}\frac{\eta(\mathbf{r}')}{|\mathbf{r}-\mathbf{r}'|}d\Gamma \tag{7}$$

and

$$\phi^-(\mathbf{r}) = \int_D \frac{1}{4\pi\sigma_-}\frac{\mathbf{P}(\mathbf{r}')\cdot(\mathbf{r}-\mathbf{r}')}{|\mathbf{r}-\mathbf{r}'|^3}d\mathbf{r}' + \sum_{i=1}^{M}\oint_{S_i}\frac{1}{4\pi\epsilon_-}\frac{\eta(\mathbf{r}')}{|\mathbf{r}-\mathbf{r}'|}dS_i + \oint_\Gamma \frac{1}{4\pi\epsilon_-}\frac{\eta(\mathbf{r}')}{|\mathbf{r}-\mathbf{r}'|}d\Gamma \tag{8}$$

where the the domain of ϕ^+ is B and the domain of ϕ^- is M.

As expected, the ${K_{i,j}}^+$s act as follows:

$${K_{i,j}}^+(\rho_i) = \oint_{S_i}\frac{1}{4\pi\epsilon_+}\frac{\rho_i(\mathbf{r}')}{|\mathbf{r}-\mathbf{r}'|}dS_i \text{ with domain } \mathbf{r}\,\epsilon\, S_j.$$

The + simply emphasizes that $\mathbf{r}$ is restricted to B. Likewise, the ${M_i}^+$s are defined for the integrals over Γ, the interface.

Furthermore, the top row of the matrix L_{inh} contains normal derivative operators described by the notation

$$\frac{\partial}{\partial\mathbf{n}}({K_i}^{+,-}) = \frac{\partial}{\partial\mathbf{n}}({K_i}^+ + k{K_i}^-). \tag{9}$$

${K_i}^+$ is the same as ${K_{i,j}}^+$ with the looser domain restriction $\mathbf{r}\,\epsilon\,B$ (K_i^- is symmetrically defined on M). Likewise, the operators M^+ and M^- represent looser domain restrictions of their counterparts in the middle E rows of L_{inh} to B and M, respectively. Note that in the expression above, the normal vectors to Γ used for the computing the directional derivatives for the + and - operators have opposite orientations.

For computational purposes, it is comparatively easy to take the normal derivative of the first two terms of the right-hand sides of the potential equations (7) and (8). The only matter of concern is how to apply the normal derivative to the surface integral terms over Γ. The reader should verify that the normal derivative operator passes through the third term, adding or subtracting $\eta/2$, depending if $\mathbf{r}\epsilon B$ or M, respectively.

3.3 The Operators in Terms of Basis Functions

The weighting scheme is as before, except for the + and - subscripts. We take this into account with a coefficient, $\Delta(\mathbf{r})$ which reminds us that there are two domains: the blood and the myocardium. For convenience, we define ${J_i}^+ = \int_D \frac{1}{4\pi\sigma_+}\frac{\mathbf{P}(\mathbf{r}')\cdot(\mathbf{r}-\mathbf{r}')}{|\mathbf{r}-\mathbf{r}'|^3}d\mathbf{r}'$ subject to the condition that $\mathbf{r}\epsilon S_i$. Continuing, we write

$$< u(\mathbf{r}), v(\mathbf{r}) >= \int_{R^3}\Delta(\mathbf{r})u(\mathbf{r})v(\mathbf{r})\; d\mathbf{r}.$$

Then when m travels over the jth surface, we show (as before) that the value of $g_{j,m}$ is

$$g_{j,m} =< w_{j,m}, g >= \int_{R^3}\Delta(\mathbf{r})\delta(\mathbf{r}-\mathbf{r_{j,m}})g(\mathbf{r})\; d\mathbf{r} = -{J_i}^+,$$

depending on the surface element to which $\mathbf{r_{j,m}}$ belongs.

3.4 Physical Derivation

The structure of L_{inh} is based on the physical properties that we want to satisfy. First, we want $\Delta\phi^+ = 0$ on $B - \cup_{i=1}^{E} S_i$ and also, $\Delta\phi^- = 0$ on $M - D$. This suggests a boundary condition on the normal derivatives (where $\mathbf{n}$ is the normal vector to Γ evaluated pointwise on this 2-manifold). This flux condition is given by

$$\frac{\partial\phi^+}{\partial\mathbf{n}} = k(\mathbf{r})\frac{\partial\phi^-}{\partial\mathbf{n}}.$$

Here, $k(\mathbf{r})$ depends on the geometric conformation of Γ, but the requirement that charge collects on Γ forces $sign(k(\mathbf{r})) = sign(k(\mathbf{r}''))$ for each $\mathbf{r}''$ distinct from $\mathbf{r}$.

A look at the operator matrix shows that the above flux equation is represented by a row of L_{inh}, but that a continuity equation seems absent. To skirt the continuity issue, we take the forms for ϕ^+ and ϕ^- to have identical coefficients (that is, $\sigma_+ = \sigma_-, \epsilon_+ = \epsilon_-$). This choice guarantees that $\phi^+|\Gamma = \phi^-|\Gamma$. We make up the difference by defining $k(r) = (\sigma_+/\sigma_-)H(\mathbf{r})$ where $H(\mathbf{r})$ takes into account the geometry of Γ.

To summarize, the top row of L_{inh} comes from the normal derivative condition and the other rows represent conditions we already have from the homogeneous problem. These pre-existing conditions are just modified by the superposition of potential due to the build-up of charge on the interface Γ.

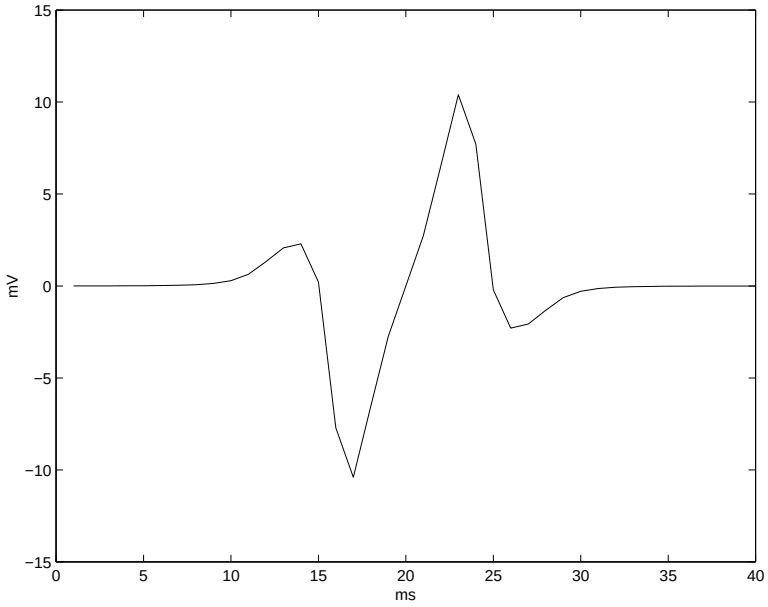

Figure 1: Response of probe in the form of a cylinder with a hemispherical tip. The distance from the tip of the electrode to the tissue is 2mm. The vertical axis is the voltage difference between the cylinder and the tip.

4 Results and Discussion

As the dipole layer moves through the myocardium, the potentials on the electrodes change. In bipolar sensing, these potentials and those on nearby electrodes are compared and plotted as functions of time, while in unipolar sensing, they are compared with an outside reference electrode. The desirability of a given electrode configuration can be measured using the near to far field ratio (*nffr*), given by

$$nffr = \frac{nearmax}{farmax}$$

where *nearmax* is the maximal amplitude of the potential difference in the near field and *farmax* is the maximal amplitude of the potential difference in the far field. In other words, *nearmax* measures the strength of the desired atrial signal, while *farmax* measures the strength of the distant ventricular signal [5].

We modulated various parameters and observed the effects on the *nffr*. For both hemispherical and cylindrical tips, we measured the *nffr*, varying the tip size and the tip-to-ring spacing (the distance between the tip and the cylindrical ring). We tested both unipolar and bipolar sensing, selecting reasonable values for all parameters which were not being changed.

With the homogeneous medium model (section 2), unipolar sensing and a hemispherical tip, the maximal *nffr* occurred at a radius of 1.4mm, while for a cylindrical tip, the maximum occurred at a radius of 1.5mm.

With the homogeneous medium model, bipolar sensing and a hemispherical tip, the tip-to-ring spacing needed to be as small as possible in order to maximize *nffr*. With a cylindrical tip, the maximal *nffr* occurred at a tip-to-ring spacing of .5mm.

Using the homogeneous medium model, bipolar sensing and a cylindrical tip, the maximal *nffr* occurred at a radius of 1.3mm.

Using the homogeneous medium model, bipolar sensing and a hemispherical tip, the *nffr* was maximized with a tip of radius 1.1mm. However, using the inhomogeneous medium model described in section 3, with all other parameters held identical to the homogeneous medium case, the *nffr* was maximized with a much smaller tip of radius .2mm. With the inhomogeneous medium model, the plot of *nffr* against tip size had two local maxima (unlike all other plots). Most surprisingly, the inhomogeneous medium model predicted that a 1.1mm tip is one of the worst choices possible. According to the more sophisticated inhomogeneous medium model, it would have been better to randomly guess a spacing distance rather than use the simpler homogeneous medium model!

These preliminary results indicate that the *nffr* is sensitive to the choice of model and to the model parameters. For bipolar sensing, varying the tip-to-ring spacing produced a much greater range of *nffr* values than other manipulations of the paramters. Further testing and refinement of the MATLAB code used for our derivations and future work with the MATLAB code are necessary for solidifying the initial predictions of the models. In the future, the use of different geometries for the electrodes and more sophisticated characterizations of the dipole wave in the myocardium, along with careful study of the new inhomogeneous model described in section 3, may lead to better electrode design.

The authors thank Shirley Min and Fernando Reitich for their valuable assistance.

References

[1] Richard F. Harrington, *Field Computation by Moment Methods.* New York: The Macmillan Company, 1977.

[2] Kaj-Åge Henneberg, and Robert Plonsey, "Boundary Element Analysis of the Directional Sensitivity of the Concentric EMG Electrode," *IEEE Transactions on Biomedical Engineering* vol. 40 no. 7, 621-631, Jul. 1993.

[3] John David Jackson, *Classical Electrodynamics.* New York: John Wiley & Sons, 1975.

[4] Yongmin Kim, and Paul H. Schimpf. "Electrical Behavior of Defibrillation and Pacing Electrodes." *Proceedings of the IEEE* vol. 84 no. 3, 446-456, Mar. 1996.

[5] Xiaoyi Min, Mark L. Brown, and Rahul Mehra, "Computer Simulation of Effect of Bipolar Electrode Tip to Ring Spacing on P Wave and Far Field R Wave Sensing in Atrium." Unpublished manuscript.

[6] Weimin Sun, and Xiaoyi Min, "An Integral Equation Model for Intracardiac Electrogram Sensing." *IEEE Transactions on Biomedical Engineering* vol. 44 no. 12, 1237-1242, Dec. 1997.